First-principles study of the electronic properties of graphite

J.-C. Charlier, X. Gonze,* and J.-P. Michenaud
Laboratoire de Physico-Chimie et de Physique des Matériaux, Université Catholique de Louvain, 1 place Croix du Sud, B-1348 Louvain-La-Neuve, Belgium
(Received 24 September 1990)

The electronic properties of hexagonal graphite have been studied in the framework of the density-functional technique, using nonlocal ionic pseudopotentials and a large number of plane waves. The valence charge density and the density of states are presented, as well as the band structure and the charge-density contributions of some typical wave functions. The electronic energies, at the Fermi level, are parametrized by the Slonczewski-Weiss-McClure model, and compared with the parametrization of experimental data. The numerical accuracy of the calculation has been controlled, in order to provide a reliable comparison between theory and experiment. In particular, the agreement obtained in the framework of the density-functional theory for electronic energies at the Fermi level is surprisingly good.

I. INTRODUCTION

Graphite is a material made of hexagonal-symmetry carbon layers that are weakly coupled to neighboring layers. Various interesting properties are related to this peculiar geometry, and, in particular, the weak overlap between valence and conduction bands that leads to its semimetallic behavior. Since the early 1950s, a variety of independent theoretical studies have established the main features of the band structure and the shape of the Fermi surface.[1] The great interest in graphite material is manifested by the vast literature dedicated to this subject. The reasons for this interest are threefold: first, this material is of great industrial interest; second, graphite has often been chosen to test theoretical methods aimed to study two-dimensional materials;[2] and third, quantum-chemistry theorists have also been interested in graphitic planes with polyaromatic molecules.[3]

The investigation of this material by precise self-consistent *ab initio* techniques has only been undertaken since the 1980s.[4] Each of these studies focused on some aspect of graphite—mainly structural properties, but also electronic properties. Let us also point out that some of these properties were well reproduced using semiempirical or non-self-consistent studies.[5]

In this paper we aim at presenting state-of-the-art *ab initio* calculations over a wide range of electronic properties: valence charge density, band structure, charge density for each band, density of states (DOS), and Fermi surface. The precision requirement is particularly stringent for this latter property. Nevertheless, we have been able to satisfactorily reproduce, within our small error bars, the experimental Fermi-surface shape and free-carrier number, which are very sensitive quantities.

In the framework of density-functional theory, according to the current understanding of the so-called "band-gap problem,"[6] such a good dealing with the other semimetallic elements[7] (arsenic, antimony, bismuth), a quite good agreement for the Fermi surfaces was also obtained. In the present study, we carry on the investigation.

The paper starts with a presentation of the atomic properties and the graphitic structure. The hexagonal graphitic crystalline state is compared with diamond (Sec. II). Then, we critically discuss the *ab initio* theoretical method that we used to study the above-mentioned properties (Sec. III): a self-consistent density-functional approach, using *ab initio* nonlocal pseudopotentials and a local-density approximation for exchange and correlation. Numerical results for the electronic properties and Fermi-surface description are presented and compared with experimental results in Secs. IV and V. Finally, we summarize this study.

II. ATOMIC PROPERTIES AND GRAPHITIC STRUCTURE

The ground-state carbon-atom configuration is $1s^2 2s^2 2p^2$. The $1s$ electrons are core electrons, and the remaining four are valence electrons. Indeed, the energies of $2s$ and $2p$ levels are found, respectively, at -13 and -5 eV below the vacuum level, while the $1s$ level is well below: -270 eV (see, for example, Ref. 8, and references contained therein).

No p electrons exist inside the core shell. As the p valence electrons do not come under the influence of repulsion due to the orthogonalization with core states,[9] the $2p$ wave function is quite localized.[8] The distance of the carbon $2p$ wave-function maximum to the nucleus is nearly the same as the carbon $2s$ wave-function maximum.

Natural carbon can be found in two allotropic forms: diamond and graphite. The bonding between atoms is different in each form, while mainly covalent. In diamond, the bonds come from the sp^3 hybridization of atomic orbitals (four bonds and angles of 109.5°). In graphite, the sp^2 (s-p_x-p_y) hybridization of atomic orbitals (denoted σ) forms a covalently bound lattice of graphitic planes (angles of 120° between the segments connecting nearest-neighbor atoms) which are piled up one on each other and weakly bound by the residual forces

that arise from the nonhybridized p_z orbitals (denoted π) perpendicular to the planes. The graphitic lattice (a) and the three-dimensional Brillouin zone (b) are presented in Fig. 1.

In a graphitic monolayer, the first four bands (σ and π) are occupied while the last four are empty. Because of symmetry properties, π (bonding) and π^+ (antibonding) bands are degenerate at the K point of the two-dimensional (2D) Brillouin zone. So the 2D graphite is a zero-gap semiconductor.[1] The interactions between graphitic planes modify this situation and create a semimetal. Nevertheless, these weak interactions can perfectly be treated as perturbation of the 2D situation.

The 3D structure of graphite is not a simple stacking of planes. Every other plane is shifted in the horizontal plane and gives the stacking noted *ABABAB* [cf. Fig. 1(a)]. This crystallographic structure belongs to the $P6_3/mmc$ space group.

Four atoms are present in the three-dimensional unit cell: two atoms for each graphitic plane and two planes per cell (*AB*). Figure 1(a) also presents this cell, which is high and narrow. At 0 K, its dimensions are $c_0=6.674$ Å, $a_0=2.4589$ Å.[10] From this, we can deduce the distance between planes (3.337 Å) and between nearest neighbors (1.420 Å).

III. THEORETICAL METHOD

We performed a quite standard Hohenberg-Kohn-Sham density-functional calculation[11] with the Ceperley-Alder exchange-correlation energy as parametrized by Perdew and Zunger.[12] The ionic-core potential was replaced by an *ab initio* norm-conserving pseudopotential, taken from the complete table of Bachelet, Hamann, and Schlüter.[13] We used a plane-wave basis set (up to 1700 plane waves, depending on the required accuracy) within the framework of the momentum-space formalism,[14] and solved the self-consistent Schrödinger equation for the band structure, using the algorithm of Wood and Zunger,[15], and a modified "simple-mixing" scheme[16] for the density self-consistency.

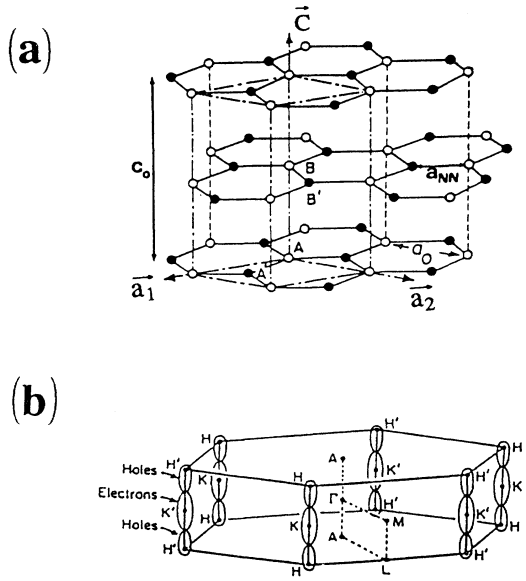

FIG. 1. (a) Crystalline structure of hexagonal graphite (Ref. 1). The dimensions of the unit cell, which is represented by dotted-dashed lines, are a_0 and c_0. a_{NN} is the distance between nearest neighbors. (b) Graphite Brillouin zone showing several high-symmetry points and a schematic version of the graphite electron and hole Fermi surfaces located along the H-K axes (Ref. 24). Each symmetric point is labeled with the usual Bouckaert-Smoluchowski-Wigner notation (Γ, A, H, K, L, M).

In connection with this treatment of semimetal electronic structure, two technical points are worth mentioning: treatment of the band occupation and Brillouin-zone-sampling procedure. Besides a complete description of the method used, an extensive study of the uncertainties associated with each numerical parameter or approximation is required. In view of the small overlap (of the order of 40 meV) between valence and conduction bands, the maximum truncation error on energies at the Fermi level has been reduced to 5 meV. At other points in the Brillouin zone, the accuracy requirement is somewhat less stringent.

The measured number of conduction electrons or valence holes is *very small* ($<1\times10^{-4}$ per atom). The theoretically calculated number is of the same order of magnitude. We have thus constructed the density of charge with complete filling of the first eight bands, treating the crystal as a semiconductor. For arsenic, antimony, and bismuth, this approximation was adequate.[7] We have also made some trials to measure the effect of this approximation in graphite: The maximal variation of the eigenvalues is less than 0.05 meV.

The number of special points[17] needed to sample the Brillouin zone is also of interest. Using symmetry, we can limit the investigated zone to a 24th of the entire Brillouin zone. To generate an estimation of the number of special points needed, we have performed a study using 14, 28, 42, 56, and 70 special points in the irreducible part of the Brillouin zone, the last number being representative of perfect accuracy. The discrepancies for 14, 28, 42, and 56 points are 20, 4.4, 1.2, and 0.4 meV, respectively. In this investigation, we use 28 special points (14 **k** points in each plane, with two planes) to obtain the self-consistent density, where the accuracy on eigenvalues (near the Fermi energy) is of great importance. For the density-of-states (DOS) calculation, we have used the Lehmann-Taut analytical tetrahedron method[18] with 198 points in an irreducible part of the Brillouin zone.

The problems inherent in the use of the density-functional formalism will be discussed more specifically in the final part of this paper.

IV. THE ELECTRONIC PROPERTIES

A. The valence charge density

The valence charge density of graphite has been calculated by the *ab initio* technique described in the preceding sections, with experimental crystalline parameters.[10] To construct the density, 797 plane waves have been used;

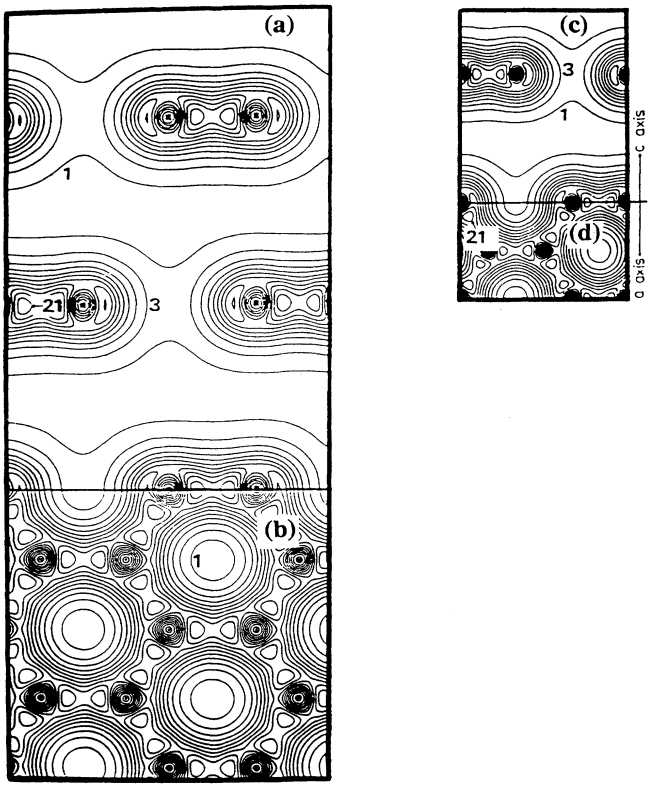

FIG. 2. Valence-electron pseudocharge density of graphite obtained *ab initio*. (a) Perpendicular to graphitic planes. (b) In the graphitic plane. The same densities of charge obtained experimentally are presented in (c) and (d) (x-ray diffraction, Ref. 19). The contour interval is in units of 0.1 electrons/Å^3 with a difference of 0.2 electrons/Å^3 between curves. Crosses indicate atoms positions.

this set of plane waves corresponds to a kinetic energy of 16.5 hartrees. The determination of the density was such that inaccuracies in eigenenergies associated with an eventual lack of self-consistency were less than 10^{-6} hartree.

Figure 2 represents the result of this calculation. The isodensity lines display the main features of binding. The absence of covalent bonds is clearly seen in the density which is perpendicular to the graphitic planes [2(a)]. However, the covalent bonds between carbon atoms are present in the in-plane density [2(b)]. The latter shows up the hexagonal symmetry whereas the former exhibits the shift between neighboring planes in the stacking. The agreement with experiment[19] (measurement of the density of charge by x-ray diffraction [2(c) and 2(d)]) is remarkable.

B. The band structure

The self-consistent calculation of the density of charge allows us to construct the band structure. Figure 3 shows the band structure in different special directions of the Brillouin zone (for the first nine or ten bands).

The comparison with the band structure of the monolayer of graphite is especially interesting. Because of the doubling of the unit cell (graphitic monolayer $\rightarrow ABAB$ stacking), each band of the bidimensional structure is split in two bands. In the A-H-L plane of the Brillouin zone of 3D graphite, the degeneracy is not lifted to any order over the entire plane because the crystallographic structure possesses a particular reversal element which is a twofold screw axis normal to the zone boundary plane.[20] So, in this A-H-L plane, the 3D structure is very similar to the monolayer band structure.

However, when we move away from this plane and go towards the middle plane of the Brillouin zone, Γ-M-K, some degeneracies are very weakly lifted (the lift of the degeneracy is nearly invisible in Fig. 3), others are more strongly lifted (see lines $K-H$, $\Gamma-K$, and $M-L$). In the case of the π band bonding (third and fourth valence bands at the Γ point), the dispersion is very strong.

This dispersion is stronger for a conduction band: the ninth band at the Γ point (detailed in Fig. 4). The wave function associated with this conduction band possesses an interesting characteristic: its density is maximum between graphitic planes and not in the plane as for all the valence bands. The position of this special band has been

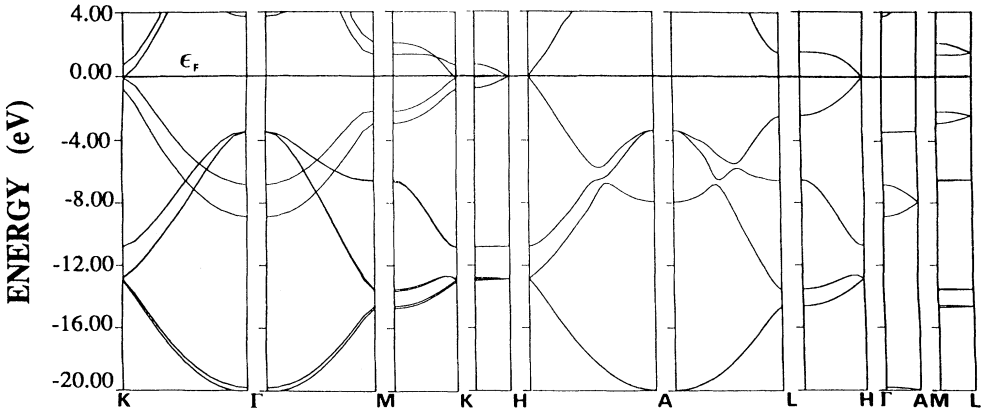

FIG. 3. *Ab initio* band structure of graphite along different lines in the Brillouin zone.

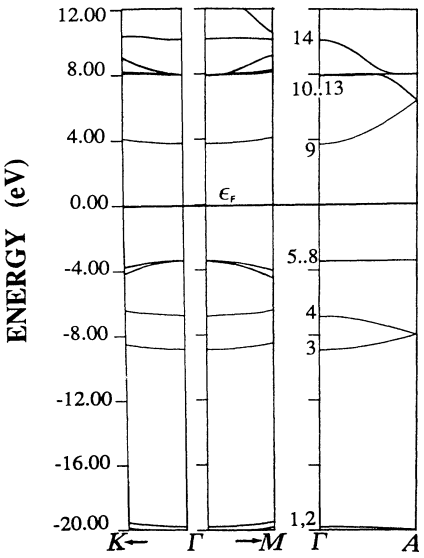

FIG. 4. The band structure is detailed around the Γ point for the first 14 bands (8 valence bands + 6 conduction bands). The dispersive character of the 3, 4, 9, and 14 bands along Γ-A is clearly distinguishable. The position of the ninth band has been discussed in many articles (see text).

discussed in many articles.[21] This band is unoccupied in pristine graphite but, in graphite intercalated with metals, the same band, eventually hybridized with the supplementary orbitals, could become occupied. This would decrease the anisotropy of the density of graphite and, in the same way, many electrical properties, because this band reduces the isolation of the graphitic planes and also because the effective mass of the electrons is smaller in the c direction than in conduction bands of nonintercalated graphite (see curvature of the end of the band, line Γ – A).

Table I compares our numerical results for energy differences with other theoretical and experimental ones. The energies around the Fermi level will be studied in the next section.

In general, the present results are consistent with the previous literature. The splitting of the bands at the K point near the Fermi level is in good agreement with experiment. The total valence-band width (20.1 eV), the σ-band width (16.7 eV) and the σ-π band separations [10.9 eV (bottom) and 3.3 eV (top)] are very close to the previous calculations. We find that the bottom of the π band is split by 2.1 eV due to interlayer interactions whereas the σ bands (which are highly concentrated near the carbon layers) are being split considerably less [0.3 eV (bottom) and 0.1 eV (top)]. These present values are consistent with the other theoretical calculations.

We can also see a large difference between the eigenvalues at the top of the σ band. These eigenvalues are very sensitive to the number of the **k** points used in the iterations (see Jansen and Freeman in Ref. 4). This could explain the error of about 1 eV for the number of **k** points used.

C. The density of states

The electron density of states (DOS), as a function of the energy, has been calculated with the tetrahedron method.[18] For this calculation, 198 **k** points in the Brillouin zone have been used (three planes of 66 **k** points each) and a kinetic energy of 21 hartrees associated with this set of planes waves.

TABLE I. Characteristic electronic energies (in eV) of graphite evaluated from the Fermi level. The first four columns are theoretical results. The last column is a collection of experimental data.

	Present work	Other theoretical			Experimental
Bottom σ	−20.1[a]	−19.6[b]	−20.8[c]	−19.5[d]	−20.6[e]
	−19.8[a]	−19.3[b]	−20.5[c]	−19.2[d]	
Bottom π	−8.9[a]	−8.7[b]	−9.1[c]	−8.2[d]	−8.1[e], −8.5[f]
	−6.8[a]	−6.7[b]	−7.1[c]	−6.5[d]	−7.2[e], −5.7[g], −6.6[f]
Top σ	−3.5[a]	−4.6[b]	−3.4[c]	−4.3[d]	−4.6[e], −5.5[f]
	−3.4[a]	−4.6[b]	−3.3[c]	−4.3[d]	
Unoccupied σ^*	3.7[a]	3.8[b]	3.7[c]	7.1[d]	
	7.9[a]	8.3[b]	9.0[c]	7.3[d]	6.9[e]
	7.9[a]	8.4[b]	9.3[c]	7.3[d]	
π bands at point K					
$\epsilon_1^0-\epsilon_3^0$	0.80[a]		0.7[c]	0.44[d]	0.72[h]
$\epsilon_3^0-\epsilon_2^0$	0.86[a]		0.8[c]	0.61[d]	0.84[h]

[a]Present work.
[b]H. J. F. Jansen and A. J. Freeman, Phys. Rev. B **35**, 8207 (1987).
[c]N. A. W. Holzwarth, S. G. Louie, and S. Rabii, Phys. Rev. B **26**, 5382 (1982).
[d]R. C. Tatar and S. Rabii, Phys. Rev. B **25**, 4126 (1982).
[e]W. Eberhardt, J. T. McGovern, E. W. Plummer, and J. E. Fischer, Phys. Rev. Lett. **44**, 200 (1980).
[f]A. R. Law, J. J. Barry, and H. P. Hughes, Phys. Rev. B **28**, 5332 (1983).
[g]A. Bianconi, S. B. M. Hagström, and R. Z. Bachrach, Phys. Rev. B **16**, 5543 (1977).
[h]G. Bellodi, A. Borghesi, G. Guizzeti, L. Nosenzo, E. Reguzzoni, and G. Sammoggia, Phys. Rev. B **12**, 5951 (1975).

The calculated DOS for the valence states is presented in Fig. 5(a). Figures 5(b) and 5(c) compare the 0.5-eV Gaussian convolution of this DOS with the experimental XPS result obtained by Bianconi, Hagström, and Bachkrach,[22] (x-ray photoemission spectroscopy, with energetic photons of 122 eV). The experimental broadening is estimated at 0.4 eV.

We clearly see a set of states of -20 to -13 eV which comes from the first two σ bands. The 2D characteristic of these two first bands which had already been seen in the lack of dispersion in accordance with the $\Gamma-A$, $M-L$, and $K-H$ lines, is confirmed by the DOS form which suddenly increases from zero to a nearly constant value. Instead of increasing as the square root of the energy (which is the behavior of the density of states for free electrons in three dimensions), the density of states is a step function which is clearly a characteristic of a two-dimensional behavior. The small oscillations around the constant value should be ascribed to the tetrahedron method.[23]

The other four σ bands and the two π bands, which overlap near the Γ point, give features in the energy interval $[-13,0]$ eV. The theory reproduces the experimental peak locations quite well. The values of the computed amplitudes are less satisfactory.

D. The partial charge densities

Many densities of charge of different wave functions for different special points of the Brillouin zone have been represented in Figs. 6 and 7. These densities of charge

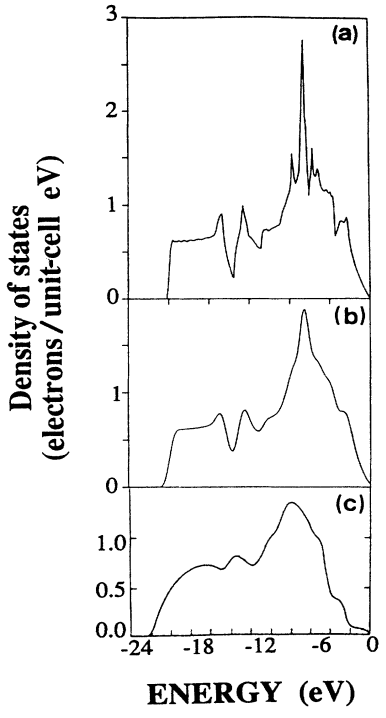

FIG. 5. Comparison of (a) theoretical density of states (DOS), (b) theoretical smoothed DOS (0.5 eV Gaussian smoothing), and (c) experimental x-ray photoemission spectra (XPS) (Ref. 22).

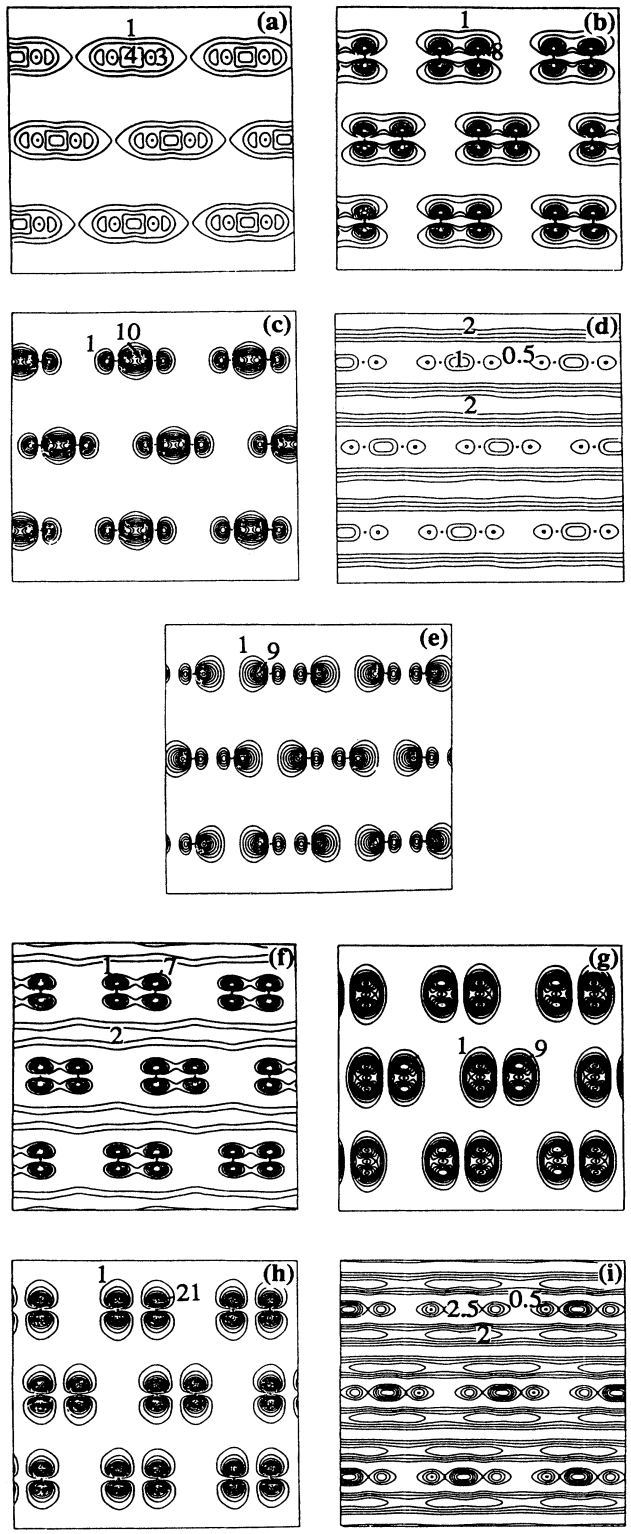

FIG. 6. Charge-density contributions of some typical wave functions at the Γ point of the Brillouin zone: (a) second band, (b) fourth band, (c) eighth band, (d) ninth band, (e) tenth band, (f) fourteenth band, (g) fifteenth band, (h) seventeenth band, (i) eighteenth band. All these densities are presented in electron/unit cell.

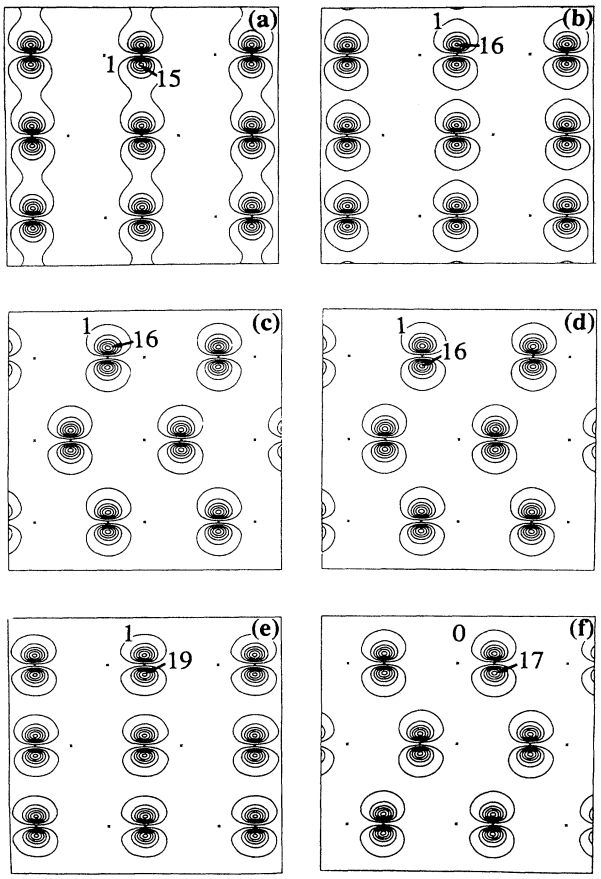

FIG. 7. Charge-density contributions of some typical wave functions at the K and H points of the Brillouin zone and at a point near H. These densities are representative of the situation around the Fermi level. (a) Seventh band at K, (b) Seventh band at H, (c) ninth band at K, (d) ninth band at H, (e) tenth band at K (electrons), (f) eighth band at 0.8 of the K-H line (holes). All these densities are presented in electron/unit cell.

(for example at the Γ point) allow a more intuitive representation of the different orbitals which are present in graphite. Figure 6(a) presents the second band at the Γ point, which is related to σ bonding (s orbital). This Figure shows the interaction between neighboring carbon atoms inside the same graphitic plane. Figure 6(b) presents the fourth band at the Γ point, which is related to π bonding (p_z orbital). This figure shows the interaction between neighboring carbon atoms outside the graphitic plane. Figure 6(c) presents the eighth band at the Γ point, which is related to σ bonding (p_x and p_y orbitals). Figure 6(d) presents the ninth band at the Γ point. As already mentioned, we can see that the maximum of the density is localized outside the graphitic plane. Figure 6(e) presents the tenth band at the Γ point, which is related to σ^* orbitals (p_x and p_y orbitals). This figure shows the repulsion between p orbitals inside the graphitic plane. Figure 6(f) presents the fourteenth band at the Γ point, which is related to π^* orbitals (p_z orbital). Figure 6(g) presents the fifteenth band at the Γ point, which is related to σ^* orbitals (mixing of s and p orbitals). Figure 6(h) presents the seventeenth band at the Γ point, which is related to π^* orbitals (p_z orbital). Finally, figure 6(i) presents the eighteenth band at the Γ point, which is a σ bonding conduction band. We can see a maximum of the density localized outside the plane, but the maximum is more important around the bond itself.

The densities of charge at the K and H points are also particularly interesting, especially those relative to the bands around the Fermi level. Some of these partial densities are illustrated in Fig. 7.

V. THE FERMI SURFACE

A. The Slonczewski-Weiss-McClure model (SWMcC)

The interactions between graphitic planes are clearly weaker than the interactions inside the plane. The s orbitals do not contribute to the level occupation near the Fermi energy. The 2D interactions only lead to a zero-gap semiconductor with linear dispersion relations at the Fermi level near the K point.

Using a $\mathbf{k}\cdot\mathbf{p}$ perturbation method. Slonczewski and Weiss[1] and McClure[1] have calculated the band structure of graphite at the Fermi level. The electronic energy spectrum near this energy can be described by a seven-parameter model: $\gamma_0,\gamma_1,\gamma_2,\gamma_3,\gamma_4,\gamma_5,\gamma_6=\Delta$. These parameters, which define the interaction energies between π orbitals from different carbon atoms inside the plane or from plane to plane, are described in the Appendix where a summary of the SWMcC model can also be found.

B. The *ab initio* Fermi surface

Table II presents the set of parameters of the SWMcC model calculated by the *ab initio* technique explained before and is compared with other theoretical and experimental results. The eigenenergies have been calculated starting from the self-consistent density of charge (see Sec. IV). The number of plane waves used varies between 1060 and 1100 (with a corresponding kinetic energy of 42 Ry). The accuracies obtained for each different value are also presented in Table II.

The global agreement with the previous calculations and the experimental results is favorable. The γ_0 parameter leads to the greatest absolute error by comparison with experimental estimations. However, this error is only 20% in relative value which is in the same order of magnitude as the other errors in the other parameters. The very small γ_2 parameter is less accurate in relative value. The error in γ_2 is troublesome because this parameter establishes the number of free carriers. The γ_1, γ_3, and γ_5 parameters are the best estimated parameters of the present work in comparison with experiment and with the other theoretical results. The negative sign of Δ is in agreement with magnetoreflection experiments (see Toy, Dresselhaus, and Dresselhaus as cited in Table II).

The value obtained for the γ_3 parameter compares well with experimental data. The linear dependance of the eigenvalue ε_3^0, going away from the K point in the horizontal plane, can be associated with this parameter. The

TABLE II. Values of the SWMcC-model parameters (in eV), of the Fermi energy (in eV) and of the number of free carriers (in $10^{18}/cm^{-3}$) in graphite. The first seven columns are theoretical results. The last column is a collection of the best experimental evaluations.

	Present work			Other theoretical				Experimental
γ_0	2.598±0.015[a]	2.92[b]		2.73[d]	2.58[e]			3.16±0.05[h]
γ_1	0.364±0.020[a]	0.27[b]	0.36[c]	0.32[d]	0.21[e]	0.25[f]	0.41[g]	0.39±0.01[i]
γ_2	−0.014±0.008[a]	−0.022[b]	−0.045[c]	−0.019[d]	−0.014[e]	0.022[f]	−0.043[g]	−0.020±0.002[j]
γ_3	0.319±0.020[a]	0.14[b]		0.29[d]	0.026[e]			0.315±0.015[k]
γ_4	0.177±0.025[a]	0.10[b]		0.15[d]	−0.035[e]			0.044±0.024[l]
γ_5	0.036±0.013[a]	0.0063[b]	−0.004[c]	0.021[d]	−0.014[e]	−0.003[f]	0.033[g]	0.038±0.005[i]
γ_6	−0.026±0.010[a]	0.0079[b]	0.0009[c]	−0.017[d]	0.081[e]	0.09[f]	0.42[g]	−0.008±0.002[h]
ε_F	−0.013±0.008[a]	−0.027[b]		−0.022[d]	−0.015[e]			−0.024±0.002[l]
n	1.4±0.8[a]	2.3[b]		2.0[d]	1.9[e]		2.3[g]	

[a]Present work.
[b]R. C. Tatar and S. Rabii, Phys. Rev. B **25**, 4126 (1982).
[c]C. Mallet, J. Phys. C **14**, L213 (1981).
[d]H. Nagayoshi, K. Nakao, and Y. Uemura, J. Phys. Soc. Jpn. **14**, 1480 (1976).
[e]M. Tsukada, K. Nakao, Y. Uemura, and S. Nagai, J. Phys. Soc. Jpn. **32**, 54 (1972).
[f]G. S. Painter and D. E. Ellis, Phys. Rev. B **1**, 4747 (1970).
[g]W. van Haeringen and H. G. Junginger, Solid State Commun. **7**, 1723 (1969).
[h]W. W. Toy, M. S. Dresselhaus, and G. Dresselhaus, Phys. Rev. B **15**, 4077 (1977).
[i]A. Misu, E. Mendez, and M. S. Dresselhaus, J. Phys. Soc. Jpn. **47**, 199 (1979).
[j]D. E. Soule, J. W. McClure, and L. B. Smith, Phys. Rev. **134A**, 453 (1964).
[k]R. E. Doezema, W. R. Datars, H. Schaber, and A. Van Schyndel, Phys. Rev. B **19**, 4224 (1979).
[l]E. Mendez, A. Misu, and M. S. Dresselhaus, Phys. Rev. B **21**, 827 (1980).

linear dispersion relation from point K to point Γ is presented in Fig. 8. This figure also shows the band structure around the Fermi level for a set of five different directions in an interval of $[-1.5, 1.5]$ eV. Figure 9 is a detail of the same band structure but closer to the Fermi level in the energy interval $[-0.15, 0.15]$ eV. The band structure obtained is in good agreement with the experimental observations.

The precision requirements on γ_4 and γ_5 need not to be very strong because these two parameters are not very important in the SWMcC model.

On the other hand, the sign of the γ_2 parameter is of primary importance. For $\gamma_2 < 0$, the extrema relative to the electrons are localized at the K points which are the centers of small longer pockets in accordance with the $H-K-H$ edge. Above and below these pockets, two small pockets of holes are symmetrically situated. The centers of these hole pockets are nearly localized on H. The general form of the Fermi surface is represented in Fig. 1(b). This surface includes a horizontal mirror plane, three vertical mirror planes, and a trigonal symmetry axis ($H-K-H$).

The extremities of the experimental Fermi surface are found to go out of the Brillouin zone. This little dome composed of minority holes must be split up from the main hole pocket which contains majority holes. However, in the case of our set of parameters, $\gamma_2 < 0$, $\Delta < 0$, and $|\Delta| > E_F$, the limits of the Fermi surface do not go out of

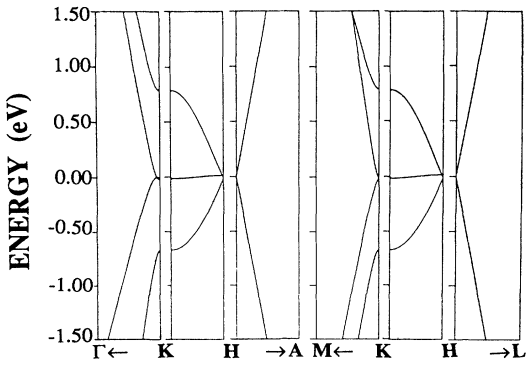

FIG. 8. The band structure around the Fermi level is detailed in the interval $[-1.5, 1.5]$ eV. The arrows show the direction away from the K-H axis. The distances shown are, respectively, $\frac{1}{3}$ of the distance from K to Γ and from H to A, and $\frac{2}{3}$ of the distance from K to M and from H to L.

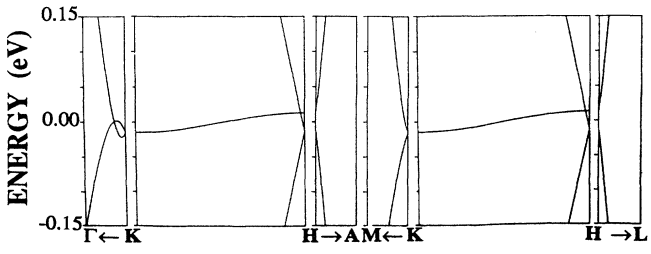

FIG. 9. The band structure around the Fermi level is detailed in the interval $[-0.15, 0.15]$ eV. The arrows show the direction away from the K-H axis. The distances shown are, respectively, $\frac{1}{15}$ of the distance from K to Γ and from H to A, and $\frac{2}{15}$ of the distance from K to M and from H to L.

the Brillouin zone and so we do not have any "minority" holes. Nevertheless a slight modification of our SWMcC parameters in their accuracy range would lead to minority carriers. In this respect, our calculations, while already very accurate, are not yet completely satisfactory.

The Fermi surface obtained from *ab initio* parameters is presented in Fig. 10. This figure shows many cuts according to different planes. This Fermi surface is composed of two pockets of majority holes, one main pocket of majority electrons, and three small pockets of minority electrons.

The influence of different parameters on the Fermi surface has also been studied. In the absence of interaction between an A atom and its neighboring B atom outside the graphitic plane, the Fermi surface would have been cylindrical. But, when the γ_3 parameter increases, the cylindrical symmetry breaks down and is reduced to a trigonal symmetry. This simulation has been numerically realized by increasing the value of γ_3 from 0 to 0.319 eV (which is the value obtained in this present work) and presented in Fig. 11.

The influence of the γ_2 parameter on the Fermi surface is shown in Fig. 12. An equienergy line has been calculated with our value, $\gamma_2=-0.014$ eV, and another one with the experimental result (-0.02 eV) of Dresselhaus *et al.*[24] In this latter result, compared to ours, the increase of $|\gamma_2|$ enhances the density of free carriers as shown in the figure. This phenomenon entails that the main pocket of electrons is going to incorporate the little pockets of minority electrons which are obtained with our set of parameters. A small modification of about 6 meV of the value of γ_2 creates minority holes and produces the disappearance of the pockets of minority electrons. This modification is within the interval of accuracy for the parameter's value.

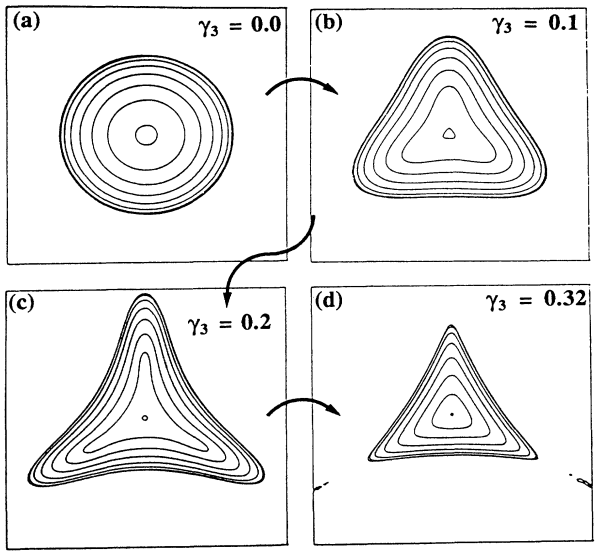

FIG. 11. Cuts in the Fermi surface of graphite showing the influence of γ_3 on the symmetry of this surface. These cuts are parallel to the graphitic planes and the vertical of the graph is the K-Γ direction. (a) $\gamma_3=0.0$ eV, (b) $\gamma_3=0.1$ eV, (c) $\gamma_3=0.2$ eV, and (d) $\gamma_3=0.319$ eV.

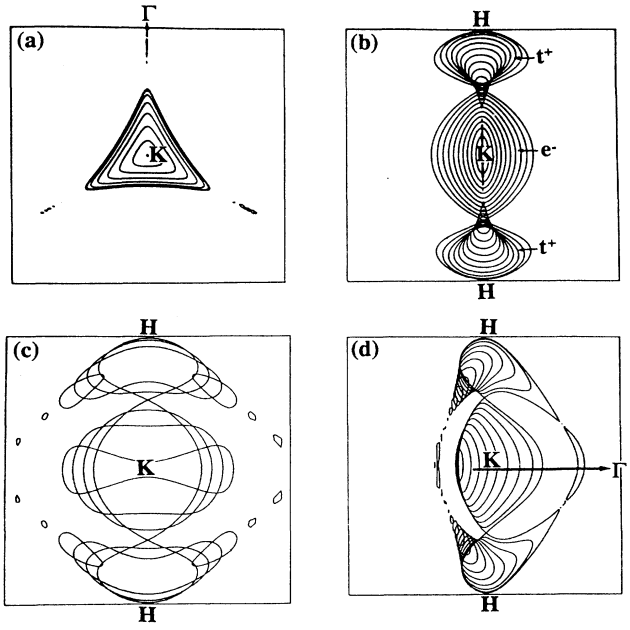

FIG. 10. Cuts in the Fermi surface of graphite which have been obtained with the set of SWMcC parameters calculated by *ab initio* techniques. (a) Cuts parallel to the graphitic planes. (b) Cuts perpendicular to the graphitic planes and to the K-Γ direction and moved sequentially towards Γ. (c) Cuts perpendicular to the graphitic planes and to the K-Γ direction and moved sequentially away from Γ. (d) Cuts perpendicular to the graphitic planes and performed in the direction perpendicular to the H-K-Γ plane. The between interval is (a) 0.06 a.u. and (b)–(d) 0.004 a.u.

The value of the Δ is also too small. Figure 13 shows that for the experimental result of Dresselhaus *et al.*[24] for Δ, minority holes are obtained.

From these discussions, we see that the proper topology of the Fermi surface could be obtained with parameters that lie within the accuracy range of our *ab initio* determinations.

VI. DISCUSSION AND CONCLUSION

The present study is *ab initio,* except for the crystallographic parameters. Our method has been submitted to a particularly stringent test, in particular for the Fermi-surface calculation. The numerical uncertainties have been identified and, when possible, systematically reduced. In this respect, our numerical treatment of the semimetallic behavior has been shown to be adequate: graphite can be treated as a semiconductor to generate the charge density.

The electronic properties of graphite have been related to the electronic properties of the atoms, leading to a qualitative comprehension of the bonding of the crystalline solid. This bonding can be decomposed into contributions of each particular band, using the partial density

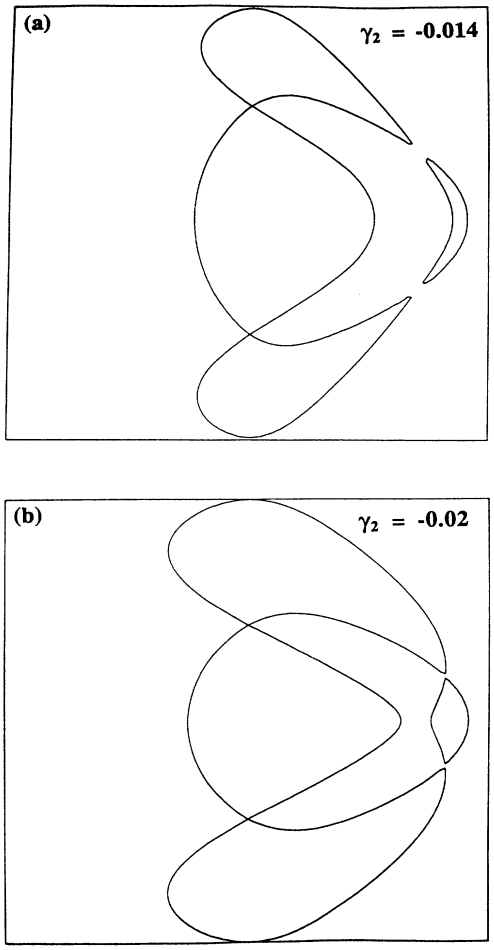

FIG. 12. Influence of the γ_2 parameter on the Fermi surface. (a) Equienergy calculated with $\gamma_2 = -0.014$ eV. (b) Equienergy calculated with $\gamma_2 = -0.02$ eV. These two cuts are the intersection of the H-K-Γ plane with the Fermi surface.

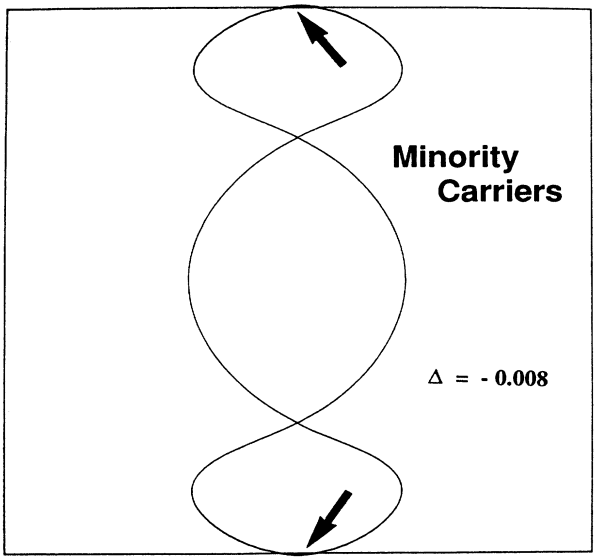

FIG. 13. Influence of the Δ parameter on the Fermi surface. Minority carriers are obtained when the value of the Δ parameter is increased to the experimental value of Dresselhaus (Refs. 1 and 24). This cut is the intersection between the Fermi surface and the plane containing the c axis and perpendicular to the $K-\Gamma$ direction.

of charge; this provides an obvious characterization of bands as bonding and antibonding σ and π bands. The band structure of graphite has been analyzed and compared with 2D case. The DOS have also been investigated, and a comparison of DOS and XPS spectra have revealed similar features: in particular, an interesting 2D character for the first two bands at the Γ point which entails a step function in a part of the DOS.

We have generated the Fermi surface of graphite, with a good qualitative result, within the achieved numerical accuracy. This fact raises some interesting questions. Within the framework of the density-functional theory, the total energy and charge density are calculated rigorously, whereas the direct identification of Kohn-Sham eigenenergies with the real band structure has little theoretical foundation. While the Fermi surface calculation from the local-density approximation (LDA) compares generally well with experiments (but can also fail even qualitatively[25]), it is well known that this approach fails to give correct values of the band gaps for semiconductors and insulators. The discrepancy between theoretical and experimental gaps is frequently of the order 0.5–1.0 eV (Ref. 6) and sometimes larger.

In the present work, we have addressed other interesting features: the shape of the Fermi surface, and the number of free carriers. From the above-mentioned failures of gap calculation, within density-functional theory, we should have expected a rather poor description of a semimetallic behavior. Moreover, some theoretical investigations have already proved the general nonequivalence between experimental and Kohn-Sham Fermi surfaces.[6] Nevertheless, we have found that a Kohn-Sham LDA calculation of graphite semimetal Fermi surface gives correct location and shape of this very small Fermi surface, and provides a good estimation of the number of free carriers. The comparison between theory and experiment is better than could have been expected from band-gap studies with the same formalism.

This study confirms the results obtained before for arsenic, antimony, and bismuth[7] and shows that the understanding of the quantitative agreement between theory and experiment is still not clear enough. Further publications will show how to understand, at least partially, the good agreement between theory and experiment for elemental semimetals (see Gonze, Ref. 1, and unpublished).

ACKNOWLEDGMENTS

We thank J. P. Vigneron, P. E. Van Camp, and V. E. Van Doren for their interest in this work. We are also

grateful to D. C. Allan for a critical reading of the manuscript. One of the authors (X.G.) has benefited from the financial support of the National Fund for Scientific Research (Belgium). This paper presents research results of the Belgian Program on Interuniversity Attraction Poles initiated by the Belgian State–Prime Minister's Office–Science Policy Programming. We also acknowledge the use of the Namur Scientific Computing Facility (Namur-SCF), a common project between the Fonds National de la Recherche Scientifique, IBM Belgium and the Facultés Universitaires Notre Dame de la Paix (FUNDP).

APPENDIX

Brief summary of the SWMcC model

The comparison between the SWMcC parameters and the atomic interactions is presented in Fig. 14.[26] The A atoms have a corresponding atom in the plane directly above or below. By contrast, B atoms have no corresponding atoms in the neighboring plane.

The γ_0 parameter represents the interaction between neighboring atoms in a graphitic monolayer. The γ_1 parameter is related to the interaction between A atoms from two neighboring graphitic planes. This parameter establishes the width of the π bands at the K point of the Brillouin zone, which is equal to $4\gamma_1$. The γ_2 parameter represents the interaction between B atoms from two next-neighbor graphitic planes. It establishes the overlapping magnitude of the π bands which is equal to $2|\gamma_2|$. The γ_3 parameter is related to the interaction between B atoms from two neighboring graphitic planes. The presence of such a coupling decreases the Hamiltonian's symmetry. The c axis becomes a threefold axis and the cylindrical symmetry of constant energy surfaces breaks into a trigonal symmetry. The γ_4 parameter is the interaction between A atom and B atom from two neighboring graphitic planes. The γ_5 parameter represents the interaction between A atoms from two next-neighboring graphitic planes. The $\gamma_6=\Delta$ parameter is the chemical-shift between A atoms and B atoms.

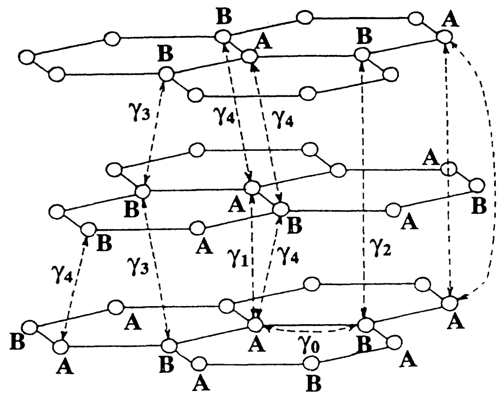

FIG. 14. Correspondence (dashed line) between the SWMcC model parameters γ_i and the interaction between the individual atoms in the graphite lattice.

The SWMcC model extends the linear dispersion law of the graphitic monolayer to the 3D case. This model is valid in some regions of the Brillouin zone, such as the neighboring of the six vertical edges $H-K-H$, and is in excellent agreement with experimental data.

Main results of the SWMcC model obtained with a k·p method

The eigenvalues of the Hamiltonian are given by the roots of the following equation:

$$(\varepsilon_1^0-\varepsilon)(\varepsilon_2^0-\varepsilon)(\varepsilon_3^0-\varepsilon)^2-\frac{\hbar^2k^2p_0^2}{m_0^2}\left[(\varepsilon_1^0-\varepsilon)(\varepsilon_3^0-\varepsilon)(1+\nu)^2+(\varepsilon_2^0-\varepsilon)(\varepsilon_3^0-\varepsilon)(1-\nu)^2+4\frac{\gamma_3^2}{\gamma_0^2}\cos^2(k_zc_0/2)(\varepsilon_1^0-\varepsilon)(\varepsilon_1^0-\varepsilon)\right]$$
$$-2\frac{\hbar^3k^3p_0^3}{m_0^3}\frac{\gamma_3}{\gamma_0}\cos(k_zc_0/2)\cos(3\alpha)[(\varepsilon_1^0-\varepsilon)(1+\nu)^2-(\varepsilon_2^0-\varepsilon)(1-\nu)^2]+\left[\frac{\hbar k p_0}{m_0}\right]^4(1+\nu)^2(1-\nu)^2=0\ ,$$

where $\nu=2(\gamma_4/\gamma_0)\cos(k_zc_0/2)$, $p_0=\frac{1}{2}\sqrt{3}(m_0/\hbar)\gamma_0a_0$ and α is the angle between the direction of the vector k and the one of the edge $H-K-H$ of the Brillouin zone.

Along a vertical axis of the Brillouin zone ($H-K-H$ or $H'-K'-H'$),

$$\varepsilon_1^0=\Delta+\gamma_1\Gamma+\tfrac{1}{2}\gamma_5\Gamma^2\ ,$$

$$\varepsilon_2^0=\Delta-\gamma_1\Gamma+\tfrac{1}{2}\gamma_5\Gamma^2\ ,$$

$$\varepsilon_3^0=\tfrac{1}{2}\gamma_2\Gamma^2\ ,$$

where Γ is defined by $2\cos(k_zc_0/2)$.

The wave vector k_z is measured from the K point; k_x and k_y at the edge H-K-H of the Brillouin zone. In the plane A-H,

$$\varepsilon_3=\tfrac{1}{2}\left[\Delta-\left\{\Delta^2+\left[\left[\frac{2\pi}{\sqrt{3}}\right]2k'\gamma_0\right]^2\right\}^{1/2}\right]\ ,$$

$$\varepsilon_1=\varepsilon_2$$
$$=\tfrac{1}{2}\left[\Delta+\left\{\Delta^2+\left[\left[\frac{2\pi}{\sqrt{3}}\right]2k'\gamma_0\right]^2\right\}^{1/2}\right]\ ,$$

$$\frac{\varepsilon_1-\varepsilon_1^0}{\Delta(k')^2}=\left.\frac{d\varepsilon}{d(k')^2}\right|_{\varepsilon=\varepsilon_1^0,k=0}$$
$$=-\left[\frac{2\pi}{\sqrt{3}}\right]^2\frac{\gamma_0^2}{\varepsilon_3-\varepsilon_1^0}(1-\nu)^2 ,$$
$$\frac{\varepsilon_2-\varepsilon_2^0}{\Delta(k')^2}=\left.\frac{d\varepsilon}{d(k')^2}\right|_{\varepsilon=\varepsilon_2^0,k=0}$$
$$=-\left[\frac{2\pi}{\sqrt{3}}\right]^2\frac{\gamma_0^2}{\varepsilon_3-\varepsilon_2^0}(1+\nu)^2 ,$$

$$\left.\frac{d\varepsilon}{dk'}\right|_{\varepsilon=\varepsilon_3^0,\ k=0}=\pm\frac{2\pi}{\sqrt{3}}\gamma_3\Gamma .$$

From these results, the calculation of the energy in three **k** points (four bands for each point) should be enough to calculate the seven parameters of the SWMcC model. Numerical inaccuracies are nevertheless present, and some more calculations are needed. On the other hand, the adequacy of the SWMcC model can be tested by these other calculations.

*Present address: Cornell University, Clark Hall, Ithaca, New York 14850.

[1]P. R. Wallace, Phys. Rev. **71**, 622 (1947); J. C. Slonczewski and P. R. Weiss, *ibid.* **99**, A636 (1955); **109**, 272 (1958); J. W. McClure, *ibid.* **108**, 612 (1957); see references in M. S. Dresselhaus, G. Dresselhaus, K. Sugihara, I. L. Spain, and H. A. Goldberg, *Graphite Fibers and Filaments,* Springer Series in Materials Science, Vol. 5 (Springer-Verlag, Berlin, 1988); N. B. Brandt, S. M. Chudinov and Ya. G. Ponomarev, *Semimetals, Graphite and its Compounds,* Modern Problems in Condensed Matter Sciences, Vol. 20.1 (North-Holland, Amsterdam, 1988); X. Gonze, thèse de doctorat, Université Catholique de Louvain, Louvain-La-Neuve, 1990.

[2]See, for example, F. Bassani and G. Pastori Parravicini, Nuovo Cimento B **50**, 95 (1967); G. S. Painter and D. E. Ellis, Phys. Rev. B **1**, 4747 (1970), and references therein.

[3]See, for example, J. M. André, L. Gouverneur, and G. Leroy, Int. J. Quantum Chem. **1**, 427 (1967); J. M. André and G. Leroy, *ibid.* **3**, 983 (1969); R. Dovesi, C. Pisani, and C. Roetti, *ibid.* **17**, 517 (1980).

[4]N. A. Holzwarth, S. G. Louie, and S. Rabii, Phys. Rev. B **26**, 5382 (1982); M. Posternak, A. Baldereschi, A. J. Freeman, E. Wimmer, and M. Weinert, Phys. Rev. Lett. **50**, 761 (1983); M. T. Yin and M. L. Cohen, Phys. Rev. B **29**, 6996 (1984); S. Fahy, S. G. Louie, and M. L. Cohen, *ibid.* **34**, 1191 (1986); **35**, 7623 (1987); H. J. F. Jansen and A. J. Freeman, *ibid.* **35**, 8207 (1987); D. Tomanek, R. M. Wentzcovitch, S. G. Louie, and M. L. Cohen, *ibid.* **37**, 3134 (1988); P. E. Van Camp, V. E. Van Doren, and J. T. Devreese (unpublished).

[5]H. Nagayoshi, K. Nakao, and Y. Uemura, J. Phys. Soc. Jpn. **41**, 1480 (1976); R. C. Tatar and S. Rabii, Phys. Rev. B **25**, 4126 (1982).

[6]M. S. Hybertsen and S. G. Louie, Phys. Rev. Lett. **55**, 1418 (1985); Phys. Rev. B **34**, 5390 (1986); R. W. Godby, M. Schlüter, and L. J. Sham, Phys. Rev. Lett. **56**, 2415 (1986); Phys. Rev. B **35**, 4170 (1987); **36**, 3497 (1987); **37**, 10159 (1988); D. Mearns, *ibid.* **38**, 5906 (1988); K. Schönhammer and O. Gunnarsson, *ibid.* **37**, 3128 (1988); N. H. March, *ibid.* **38**, 10067 (1988); J. E. Northrup, M. S. Hybertsen, and S. G. Louie, *ibid.* **39**, 8198 (1989); R. W. Godby, R. J. Needs, Phys. Rev. Lett. **62**, 1169 (1989); X. Zhu, S. Fahy and S. G. Louie, Phys. Rev. B **39**, 7840 (1989); D. Mearns and W. Kohn, *ibid.* **39**, 10669 (1989).

[7]X. Gonze, J. P. Michenaud, and J. P. Vigneron, Phys. Rev. B **41**, 11827 (1990).

[8]R. Stumpf, X. Gonze, and M. Scheffler, (Research Report of the Fritz-Haber-Institut, Berlin, 1990) (unpublished).

[9]J. C. Phillips and L. Kleinman, Phys. Rev. **116**, 287 (1959).

[10]Y. Baskin and L. Mayer, Phys. Rev. **100**, 544 (1955).

[11]P. Hohenberg and W. Kohn, Phys. Rev. **136**, B864 (1964); W. Kohn and L. J. Sham, *ibid.* **140**, A1133 (1965).

[12]D. M. Ceperley and B. J. Alder, Phys. Rev. Lett. **45**, 566 (1980); J. Perdew and A. Zunger, Phys. Rev. B **23**, 5048 (1981).

[13]G. B. Bachelet, D. R. Hamann, and M. Schlüter, Phys. Rev. B **26**, 4199 (1982).

[14]J. Ihm, A. Zunger, and M. L. Cohen, J. Phys. C **12**, 4409 (1979).

[15]D. M. Wood and A. Zunger, J. Phys. A **18**, 1343 (1985).

[16]P. H. Dederichs and R. Zeller, Phys. Rev. B **28**, 5462 (1983).

[17]H. J. Monkhorst and J. D. Pack, Phys. Rev. B **13**, 5188 (1976).

[18]G. Lehmann and M. Taut, Phys. Status Solidi B **54**, 469 (1972); P. Lambin and J.-P. Vigneron, Phys. Rev. B **29**, 3430 (1984), and references therein.

[19]R. Chen, P. Truncano, and R. F. Stewart, Acta Crystallogr. Sect. A **33**, 823 (1977).

[20]M. Lax, *Symmetry Principles in Solid State and Molecular Physics* (Wiley-Interscience, New York, 1974).

[21]M. Posternak, A. Baldereschi, A. J. Freeman, and E. Wimmer, Phys. Rev. Lett. **52**, 863 (1984); Th. Fauster, F. J. Himpsel, J. E. Fisher, and E. W. Plummer, *ibid.* **51**, 430 (1983). A precise determination of this band energy was not our aim in the present paper. We estimate that the accuracy of our calculation with respect to the relative position of this band should be of order 0.2–0.4 eV.

[22]A. Bianconi, S. B. M. Hagström, and R. Z. Bachkrach, Phys. Rev. B **16**, 5543 (1977).

[23]M. H. Boon, M. S. Methfessel, and F. M. Mueller, J. Phys. C **19**, 5337 (1986).

[24]M. S. Dresselhaus, G. Dresselhaus, K. Sugihara, I. L. Spain, and H. A. Goldberg, *Graphite Fibers and Filaments,* Springer Series in Materials Sciences, Vol. 5 (Springer-Verlag, Berlin, 1988).

[25]For metal Fermi-surface calculations, see D. D. Koelling, in *The Electronic Structure of Complex Systems,* edited by P. Phariseau and W. M. Temmerman, NATO ASI Series Vol. 113 (Plenum, New York, 1980), and references therein; A. R. Mackintosh and O. K. Andersen, in *Electrons at the Fermi Surface,* edited by M. Springford (Cambridge University Press, New York, 1980), and references therein; M. Rasolt and S. H. Vosko, Phys. Rev. Lett. **32**, 297 (1974), Phys. Rev. B **10**, 4195 (1974); Solid State Commun. **16**, 827 (1975); G. Arbman and U. von Barth, Nuovo Cimento **23B**, 37 (1974).

[26]X. Pacault, *Les Carbones* (Masson et Cie, 1965), Vol. 1.